1   # Data Supplement

2   **Sinoatrial node cell is a dynamic SYSTEM of sarcolemmal and intracellular proteins…**
3
4   Victor A. Maltsev and Edward G. Lakatta

5   Parameters and formulations of our numerical model of rabbit SANC, 4 supplemental tables, and
6   2 supplemental figures
7
8   **MATHEMATICAL DESCRIPTION OF THE MODEL**
9
10   The present model of rabbit SANC is a system of 30 first-order differential equations. All model
11   equations and parameter values are provided below. Online Table 1 summarizes all model
12   variables (y_1–y_{30}) with their initial values. The model is based on our previously published
13   version of a "Basal State" model (7) that was modified in the present study to simulate GPCR
14   modulation of rabbit SANC automaticity.
15
16   **PARAMETERS**
17
18   **Fixed ion concentrations, mM**
19    $Ca_o = 2$: Extracellular Ca^{2+} concentration.
20    $K_o = 5.4$: Extracellular K^+ concentration.
21    $K_i = 140$: Intracellular K^+ concentration.
22    $Na_o = 140$: Extracellular Na^+ concentration.
23    $Na_i = 10$: Intracellular Na^+ concentration.
24    $Mg_i = 2.5$: Intracellular Mg^{2+} concentration.
25
26   **Cell compartments**
27    $C_m = 32$ pF: Cell electric capacitance.
28    $L_{cell} = 70$ µm: Cell length.
29    $R_{cell} = 4$ µm: Cell radius.
30    $L_{sub} = 0.02$ µm: Distance between jSR and surface membrane (submembrane space).
31    $V_{cell} = \pi \cdot R_{cell}^2 \cdot L_{cell} = 3.5185838$ pL: Cell volume.
32    $V_{sub} = 2\pi \cdot L_{sub} \cdot (R_{cell} - L_{sub}/2) \cdot L_{cell} = 0.035097874$ pL: Submembrane space volume.
33    $V_{jSR\_part} = 0.0012$: Part of cell volume occupied by junctional SR.
34    $V_{jSR} = V_{jSR\_part} \cdot V_{cell}$: Volume of junctional SR (Ca^{2+} release store).
35    $V_{i\_part} = 0.46$: Part of cell volume occupied with myoplasm.
36    $V_i = V_{i\_part} \cdot V_{cell} - V_{sub}$: Myoplasmic volume.
37    $V_{nSR\_part} = 0.0116$: Part of cell volume occupied by network SR.
38    $V_{nSR} = V_{nSR\_part} \cdot V_{cell}$: Volume of network SR ($Ca^{2+}$ uptake store).
39
40   **The Nernst equation and electric potentials, mV**
41    $E_X = (RT/F) \cdot \ln([X]_o/[X]_i) = E_T \cdot \ln([X]_o/[X]_i)$, where
42   F = 96485 C/M is Faraday constant,
43   T = 310.15 K° is absolute temperature for 37°C,
44   R = 8.3144 J/(M·K°) is the universal gas constant,

45   E_T is "RT/F" factor = 26.72655 mV,

46   and $[X]_o$ and $[X]_i$ are concentrations of an ion "X" out and inside cell, respectively.

47    $E_{Na} = E_T \cdot \ln(Na_o/Na_i)$: Equilibrium potential for Na^+.

48    $E_K = E_T \cdot \ln(K_o/K_i)$: Equilibrium potential for K^+.

49    $E_{Ks} = E_T \cdot \ln[(K_o + 0.12 \cdot Na_o)/(K_i + 0.12 \cdot Na_i)]$: Reversal potential of I_{Ks}.

50    $E_{CaL} = 45$: Apparent reversal potential of I_{CaL}.

51    $E_{CaT} = 45$: Apparent reversal potential of I_{CaT}.

52    $E_{st} = 37.4$: Apparent reversal potential of I_{st}.

53

54   **Sarcolemmal ion current types and their parameter values**

55

56   I_{CaL}:   L-type Ca^{2+} current [$g_{CaL,max,basal} = 0.58$ nS/pF, as in Kurata et al. model (4)].

57   Steady-state activation parameters: $V_{½,d} = -13.5$ mV; $K_d = 6$ mV.

58   Steady-state inactivation parameters: $V_{½,f} = -35$ mV; $K_f = 7.3$ mV.

59              $K_{mfCa} = 0.00035$ mM: Dissociation constant of Ca^{2+}-dependent I_{CaL} inactivation.

60              $\beta_{fCa} = 60$ mM$^{-1} \cdot$ ms^{-1}: Ca^{2+} association rate constant for I_{CaL}.

61              $\alpha_{fCa} = 0.021$ ms^{-1}: Ca^{2+} dissociation rate constant for I_{CaL}

62              $b_{CaL,max} = 0.31$: maximum ACh-induced inhibition of I_{CaL}.

63

64   I_{CaT}:   T-type Ca^{2+} current ($g_{CaT,max} = 0.1832$ nS/pF).

65

66   I_f: Hyperpolarization-activated current ($g_{If,max} = 0.15$ nS/pF).

67              $V_{If,1/2,basal} = -64$ mV: half activation voltage for I_f current in the basal state.

68              $s_{max} = -7.2$ mV: maximum ACh-induced shift of I_f half activation voltage.

69              $n_f = 0.69$ and $K_{0.5,f} = 12.6$ nM: Michaelis-Menton parameters for ACh modulation of I_f.

70

71   I_{st}:   Sustained non-selective current ($g_{st,max} = 0.003$ nS/pF).

72

73   I_{Kr}:   Delayed rectifier K^+ current rapid component ($g_{Kr,max} = 0.08113973$ nS/pF).

74

75   I_{Ks}:   Delayed rectifier K^+ current slow component ($g_{Ks,max} = 0.0259$ nS/pF).

76

77   I_{to}:   4-aminopyridine sensitive transient K^+ current ($g_{to,max} = 0.252$ nS/pF).

78

79   I_{sus}:   4-aminopyridine sensitive sustained K^+ current ($g_{sus,max} = 0.02$ nS/pF).

80

81   I_{NaK}: Na^+/K^+ pump current ($I_{NaK,max} = 2.88$ pA/pF).

82              $K_{mKp} = 1.4$ mM: Half-maximal K_o for I_{NaK}.

83              $K_{mNap} = 14$ mM: Half-maximal Na_i for I_{NaK}.

84

85   I_{bCa}:   Background Ca^{2+} current ($g_{bCa} = 0.0006$ nS/pF).

86

87   I_{bNa}:   Background Na^+ current ($g_{bNa} = 0.00486$ nS/pF).

88

89   I_{KACh}:   Acetylcholine-activated K^+ current; $I_{KACh} = 0$, when [ACh]=0.

90              $g_{KAch,max} = 0.14241818$ nS/pF.

91
92 I_{NCX}:   Na$^+$/Ca^{2+} exchanger (NCX) current (k_{NCX} = 187.5 pA/pF).
93   K_{1ni} = 395.3: intracellular Na$^+$ binding to first site on NCX.
94   K_{2ni} = 2.289: intracellular Na$^+$ binding to second site on NCX.
95   K_{3ni} = 26.44: intracellular Na$^+$ binding to third site on NCX.
96   K_{1no} = 1628: extracellular Na$^+$ binding to first site on NCX.
97   K_{2no} = 561.4: extracellular Na$^+$ binding to second site on NCX.
98   K_{3no} = 4.663: extracellular Na$^+$ binding to third site on NCX.
99   K_{ci} = 0.0207: intracellular Ca^{2+} binding to NCX transporter.
100   K_{co} = 3.663: extracellular Ca^{2+} binding to NCX transporter.
101   K_{cni} = 26.44: intracellular Na$^+$ and Ca^{2+} simultaneous binding to NCX.
102   Q_{ci}:= 0.1369: intracellular Ca^{2+} occlusion reaction of NCX.
103   Q_{co}=0: extracellular Ca^{2+} occlusion reaction of NCX.
104   Q_n= 0.4315: Na$^+$ occlusion reactions of NCX.
105
106 **Ca^{2+} diffusion**
107 τ_{difCa} = 0.04 ms: Time constant of Ca^{2+} diffusion from the submembrane to myoplasm.
108 τ_{tr} = 40 ms: Time constant for Ca^{2+} transfer from the network to junctional SR.
109
110 **SR Ca^{2+} ATPase function**
111 K_{up} = 0.6·10^{-3} mM: Half-maximal Ca$_i$ for Ca^{2+} uptake in the network SR.
112 $P_{up,basal}$ = 0.012 mM/ms: Rate constant for Ca^{2+} uptake by the Ca^{2+} pump in the network SR
113 (Please note that while we performed j_{up} computations in mM/ms, our results of parametric
114 sensitivity analysis in main text and Supplemental Tables are presented in mM/s).
115
116 **RyR function**
117 k_{oCa} = 10 mM^{-2}· ms^{-1}; k_{om} = 0.06 ms^{-1}; k_{iCa} = 0.5 mM^{-1}· ms^{-1} ; k_{im} = 0.005 ms^{-1}; EC_{50_SR} = 0.45
118 mM; k_s = 250·10^3 ms^{-1}; $MaxSR$ =15; $MinSR$ =1; HSR = 2.5;
119
120 **Ca^{2+} and Mg^{2+} buffering**
121 k_{bCM}=0.542 ms^{-1}: Ca^{2+} dissociation constant for calmodulin.
122 k_{bCQ}=0.445 ms^{-1}: Ca^{2+} dissociation constant for calsequestrin.
123 k_{bTC}=0.446 ms^{-1}: Ca^{2+} dissociation constant for the troponin-Ca^{2+} site.
124 k_{bTMC}=0.00751 ms^{-1}: Ca^{2+} dissociation constant for the troponin-Mg^{2+} site.
125 k_{bTMM}=0.751 ms^{-1}: Mg^{2+} dissociation constant for the troponin-Mg^{2+} site.
126 k_{fCM}=227.7 mM^{-1}· ms^{-1}: Ca^{2+} association constant for calmodulin.
127 k_{fCQ}=0.534 mM^{-1}· ms^{-1}: Ca^{2+} association constant for calsequestrin.
128 k_{fTC}=88.8 mM/ms: Ca^{2+} association constant for troponin.
129 k_{fTMC}=227.7 mM/ms: Ca^{2+} association constant for the troponin-Mg^{2+} site.
130 k_{fTMM}=2.277 mM/ms: Mg^{2+} association constant for the troponin-Mg^{2+} site.
131 TC_{tot}=0.031 mM: Total concentration of the troponin-Ca^{2+} site.
132 TMC_{tot}=0.062 mM: Total concentration of the troponin-Mg^{2+} site.
133 CQ_{tot}=10 mM: Total calsequestrin concentration.
134 CM_{tot}=0.045 mM: Total calmodulin concentration.
135
136

137   **FORMULATIONS: ELECTROPHYSIOLOGY**

138

139 **Membrane potential, V_m (variable y_{15}, see Table S1 for all variables and their initial values)**

140 $dV_m/dt = - (I_{CaL} + I_{CaT} + I_f + I_{st} + I_{Kr} + I_{Ks} + I_{to} + I_{sus} + I_{NaK} + I_{NCX} + I_{bCa} + I_{bNa} + I_{KACh}) /C_m$

141

142 **Gating variables ($y_{16} - y_{30}$) and their differential equations**

143

144                         $dy_i/dt = (y_{i,\infty} - y)/\tau_{yi}$

145              $(y_i = d_L, f_L, f_{Ca}, d_T, f_T, p_{aF}, p_{aS}, p_i, n, q, r, y, q_a, q_i, a)$

146

147 τ_{yi}: Time constant for a gating variable y_i.

148 α_{yi} and β_{yi}: Opening and closing rates for channel gating.

149 $y_{i,\infty}$: Steady-state curve for a gating variable y_i.

150

151 **Ion currents**

152

153 **L-type Ca^{2+} current (I_{CaL}),** based on formulations of Kurata et al. (4) that include Ca^{2+}

154 dependent I_{CaL} inactivation. See also Table S2 for comparison of steady-state activation

155 parameters with those in other SANC models. The fractional block (b_{CaL}) of I_{CaL} by ChR

156 stimulation was adopted from (15).

157                    $I_{CaL}=C_m \cdot g_{CaL,max} \cdot (V_m - E_{CaL}) \cdot d_L \cdot f_L \cdot f_{Ca}$

158                    $d_{L,\infty}=1/\{1+ \exp[-(V_m - V_{\frac{1}{2},d})/ K_d]\}$

159                    $f_{L,\infty}=1/\{1+\exp[(V_m - V_{\frac{1}{2},f})/ K_f]\}$

160 $\alpha_{dL} = -0.02839 \cdot (V_m + 35)/ \{\exp[-(V_m+35)/2.5] - 1\} -0.0849 \cdot V_m / [\exp(-V_m/4.8) - 1]$

161                    $\beta_{dL} = 0.01143 \cdot (V_m - 5)/ \{\exp[(V_m - 5)/2.5] -1\}$

162                         $\tau_{dL} =1/(\alpha_{dL} + \beta_{dL})$

163                    $\tau_{fL} = 257.1 \cdot \exp\{-[(V_m + 32.5)/13.9]^2 \}+ 44.3$

164                         $f_{Ca,\infty}=K_{mfCa} / (K_{mfCa} + Ca_{sub})$

165                         $\tau_{fCa} = f_{Ca,\infty} / \alpha_{fCa}$

166                    $g_{CaL,max} =C_m \cdot g_{CaL,basal} \cdot (1 - b_{CaL})$

167              $b_{CaL} = b_{CaL,max} \cdot [ACh]/(K_{0.5,CaL} + [ACh])$

168

169

170 **T-type Ca^{2+} current (I_{CaT}),** based on formulations suggested by Demir et al., (2) and modified

171 by Kurata et al. (4).

172                    $I_{CaT} = C_m \cdot g_{CaT,max} \cdot (V_m - E_{CaT}) \cdot d_T \cdot f_T$

173                    $d_{T,\infty}=1/ \{1 + \exp[-(V_m + 26.3)/6.0]\}$

174                    $f_{T,\infty} = 1/\{1+ \exp[(V_m + 61.7)/5.6]\}$

175          $\tau_{dT} = 1/\{1.068 \cdot \exp[(V_m + 26.3)/30] + 1.068 \cdot \exp[-(V_m + 26.3)/30]\}$

176          $\tau_{fT} =1/\{0.0153 \cdot \exp[- (V_m + 61.7)/83.3] + 0.015 \cdot \exp[(V_m + 61.7)/15.38]\}$

177

178

179

180

181 **Rapidly activating delayed rectifier K$^+$ current (I_{Kr})**, based on formulations suggested by
182 Zhang et al. (14) and modified by Kurata et al. (4).
183

$$I_{Kr} = C_m \cdot g_{Kr,max} \cdot (V_m - E_K) \cdot (0.6 \cdot p_{aF} + 0.4 \cdot p_{aS}) \cdot p_i$$
184
$$p_{a,\infty} = 1/ \{1 + \exp[-(V_m+23.2)/10.6]\}$$
185
$$p_{i,\infty} = 1/ \{1 + \exp[(V_m + 28.6)/17.1]\}$$
186
$$\tau_{paF} = 0.84655354/[0.0372 \cdot \exp(V_m/15.9) + 0.00096 \cdot \exp(-V_m/22.5)]$$
187
$$\tau_{paS} = 0.84655354/[0.0042 \cdot \exp(V_m/17.0) + 0.00015 \cdot \exp(-V_m/21.6)]$$
188
$$\tau_{pi} = 1/[0.1 \cdot \exp(-V_m/54.645) + 0.656 \cdot \exp(V_m/106.157)]$$
189
190

191 **Slowly activating delayed rectifier K$^+$ current (I_{Ks})**, based on formulations suggested by
192 Zhang et al. (14).
$$I_{Ks} = C_m \cdot g_{Ks,max} \cdot (V_m - E_{Ks}) \cdot n^2$$
193
$$\alpha_n = 0.014/ \{1 + \exp[-(V_m - 40)/9]\}$$
194
$$\beta_n = 0.001 \cdot \exp(-V_m/45)$$
195
$$n_\infty = \alpha_n/(\alpha_n + \beta_n)$$
196
$$\tau_n = 1/(\alpha_n + \beta_n)$$
197
198

199 **4-aminopyridine-sensitive currents ($I_{4AP} = I_{to} + I_{sus}$)**, based on formulations suggested by
200 Zhang et al. (14).
$$I_{to} = C_m \cdot g_{to,max} \cdot (V_m - E_K) \cdot q \cdot r$$
201
$$I_{sus} = C_m \cdot g_{sus,max} \cdot (V_m - E_K) \cdot r$$
202
$$q_\infty = 1/\{1 + \exp[(V_m + 49)/13]\}$$
203
$$r_\infty = 1/\{1 + \exp[-(V_m - 19.3)/15]\}$$
204
$$\tau_q = 39.102/\{0.57 \cdot \exp[-0.08 \cdot (V_m+44)] + 0.065 \cdot \exp[0.1 \cdot (V_m+45.93)]\} + 6.06$$
205
$$\tau_r = 14.40516/\{1.037 \cdot \exp[0.09 \cdot (V_m+30.61)] + 0.369 \cdot \exp[-0.12 \cdot (V_m+23.84)]\} + 2.75352$$
206
207
208

209 **Hyperpolarization-activated, "funny" current (I_f)**, based on formulations of Wilders at al.
210 (13) and Kurata et al.(4). The shift s (in mV) of the I_f activation curve by ChR stimulation was
211 adopted from (15).
$$I_f = I_{fNa} + I_{fK}$$
212
$$y_\infty = 1/\{1 + \exp[(V_m - V_{If,1/2})/13.5]\}$$
213
$$\tau_y = 0.7166529/\{\exp[-(V_m + 386.9)/45.302] + \exp[(V_m - 73.08)/19.231]\}$$
214
$$I_{fNa} = C_m \cdot 0.3833 \cdot g_{If,max} \cdot (V_m - E_{Na}) \cdot y^2$$
215
$$I_{fK} = C_m \cdot 0.6167 \cdot g_{If,max} \cdot (V_m - E_K) \cdot y^2$$
216
$$V_{If,1/2} = V_{If,1/2,basal} + s$$
217
$$s = s_{max}[ACh]^{n_f} /(K_{0.5,f}^{n_f} + [ACh]^{n_f})$$
218
219

220 **Sustained inward current (I_{st})**, based on formulations of Shinigawa et al. (10) which were
221 adopted for rabbit SANC by Kurata et al. (4).
$$I_{st} = C_m \cdot g_{st,max} \cdot (V_m - E_{st}) \cdot q_a \cdot q_i$$
222
$$q_{a,\infty} = 1/\{1 + \exp[-(V_m + 57)/5]\}$$
223
$$\alpha_{qa} = 1/\{0.15 \cdot \exp(-V_m/11) + 0.2 \cdot \exp(-V_m/700)\}$$
224
$$\beta_{qa} = 1/\{16 \cdot \exp(V_m/8) + 15 \cdot \exp(V_m/50)\}$$
225

226 $$\tau_{qa} = 1/(\alpha_{qa} + \beta_{qa})$$

227 $$\alpha_{qi} = 1/\{3100 \cdot \exp(V_m/13) + 700 \cdot \exp(V_m/70)\}$$

228 $$\beta_{qi} = 1/\{95 \cdot \exp(-V_m/10) + 50 \cdot \exp(-V_m/700)\} + 0.000229/[1 + \exp(-V_m/5)]$$

229 $$\tau_{qi} = 6.65/(\alpha_{qi} + \beta_{qi})$$

230 $$q_{i,\infty} = \alpha_{qi}/(\alpha_{qi} + \beta_{qi})$$

231

232 Na$^+$-dependent background current (I_{bNa})

233 $$I_{b,Na} = C_m \cdot g_{bNa} \cdot (V_m - E_{Na})$$

234

235 Na$^+$-K$^+$ pump current (I_{NaK}), based on formulations on Kurata et al. (4), which were in turn
236 based on the experimental work of Sakai et al. (8) for rabbit SANC.

237

238 $$I_{NaK} = C_m \cdot I_{NaK,max} \cdot \{1+(K_{mKp}/K_o)^{1.2}\}^{-1} \cdot \{1+(K_{mNap}/Na_i)^{1.3}\}^{-1} \cdot \{1+\exp[-(V_m- E_{Na}+120)/30]\}^{-1}$$

239

240 Ca^{2+}- background current (I_{bCa})

241 $$I_{bCa} = C_m \cdot g_{bCa} \cdot (V_m - E_{CaL})$$

242

243

244 Na$^+$-Ca^{2+} exchanger current (I_{NCX}), based on original formulations from Dokos et al. (3).

245

246 $$I_{NCX} = C_m \cdot k_{NCX} \cdot (k_{21} \cdot x_2 - k_{12} \cdot x_1) / (x_1 + x_2 + x_3 + x_4)$$

247 $$d_o = 1+(Ca_o/K_{co}) \cdot \{1+\exp(Q_{co} \cdot V_m/E_T)\}+(Na_o/K_{1no}) \cdot \{1+(Na_o/K_{2no}) \cdot (1+Na_o/K_{3no})\}$$

248 $$k_{43} = Na_i/(K_{3ni} +Na_i)$$

249 $$k_{41} = \exp[-Q_n \cdot V_m/(2E_T)]$$

250 $$k_{34} = Na_o/(K_{3no}+Na_o)$$

251 $$k_{21} = (Ca_o/K_{co}) \cdot \exp(Q_{co} \cdot V_m/E_T) /d_o$$

252 $$k_{23} = (Na_o/K_{1no}) \cdot (Na_o/K_{2no}) \cdot (1+Na_o/K_{3no}) \cdot \exp[-Q_n \cdot V_m/(2E_T)]/d_o$$

253 $$k_{32} = \exp[Q_n \cdot V_m/(2E_T)]$$

254 $$x_1 = k_{34} \cdot k_{41} \cdot (k_{23} + k_{21}) + k_{21} \cdot k_{32} \cdot (k_{43} + k_{41})$$

255 $$d_i = 1+(Ca_{sub}/K_{ci}) \cdot \{1+\exp(-Q_{ci} \cdot V_m/E_T)+Na_i/K_{cni}\}+(Na_i/K_{1ni}) \cdot \{1+(Na_i/K_{2ni}) \cdot (1+Na_i/K_{3ni})\}$$

256 $$k_{12} = (Ca_{sub}/K_{ci}) \cdot \exp(-Q_{ci} \cdot V_m/E_T)/d_i$$

257 $$k_{14} = (Na_i/K_{1ni}) \cdot (Na_i/K_{2ni}) \cdot (1 +Na_i/K_{3ni}) \cdot \exp[Q_n \cdot V_m/(2E_T)]/d_i$$

258 $$x_2 = k_{43} \cdot k_{32} \cdot (k_{14} + k_{12}) + k_{41} \cdot k_{12} \cdot k_{34} + k_{32})$$

259 $$x_3 = k_{43} \cdot k_{14} \cdot (k_{23} + k_{21}) + k_{12} \cdot k_{23} \cdot (k_{43} + k_{41})$$

260 $$x_4 = k_{34} \cdot k_{23} \cdot (k_{14} + k_{12}) + k_{21} \cdot k_{14} \cdot (k_{34}+ k_{32})$$

261

262 Acetylcholine-activated K$^+$ current (I_{KACh}), adopted from (1) (Note I_{KACh} = 0 when [ACh]=0)

263

264 $$I_{KACh} = a \cdot g_{KACh,max} \cdot (V_m - E_K)$$

265 $$beta = 0.001 \cdot 12.32/(1+0.0042/[ACh]) \text{ (per ms)}$$

266 $$alfa = 0.001 \cdot 17 \cdot \exp(0.0133 \cdot (V_m+40)) \text{ (per ms)}$$

267 $$a_\infty = beta / (alfa + beta)$$

268 $$\tau_a = 1/(alfa + beta) \text{ (in ms)}$$

269

270

271

272

273   **FORMULATIONS: Ca^{2+} CYCLING**

274

275   **Ca^{2+} release flux ($j_{SRCarel}$) from SR via RyRs**, based on original formulations of Stern et al. (11)

276   and modified by Shannon et al. (9)

277   $$j_{SRCarel} = k_s \cdot O \cdot (Ca_{jSR} - Ca_{sub})$$

278   $$k_{CaSR} = MaxSR - (MaxSR - MinSR)/(1 + (EC_{50\_SR}/Ca_{jSR})^{HSR})$$

279   $$k_{oSRCa} = k_{oCa}/k_{CaSR}$$

280   $$k_{iSRCa} = k_{iCa} \cdot k_{CaSR}$$

281   $$dR/dt = (k_{im} \cdot RI - k_{iSRCa} \cdot Ca_{sub} \cdot R) - (k_{oSRCa} \cdot Ca_{sub}^2 \cdot R - k_{om} \cdot O)$$

282   $$dO/dt = (k_{oSRCa} \cdot Ca_{sub}^2 \cdot R - k_{om} \cdot O) - (k_{iSRCa} \cdot Ca_{sub} \cdot O - k_{im} \cdot I)$$

283   $$dI/dt = (k_{iSRCa} \cdot Ca_{sub} \cdot O - k_{im} \cdot I) - (k_{om} \cdot I - k_{oSRCa} \cdot Ca_{sub}^2 \cdot RI)$$

284   $$dRI/dt = (k_{om} \cdot I - k_{oSRCa} \cdot Ca_{sub}^2 \cdot RI) - (k_{im} \cdot RI - k_{iSRCa} \cdot Ca_{sub} \cdot R)$$

285

286   **Intracellular Ca^{2+} fluxes**

287   **Ca^{2+} diffusion flux (j_{Ca_dif})** from submembrane space to myoplasm:

288   $$j_{Ca\_dif} = (Ca_{sub} - Ca_i)/\tau_{difCa}$$

289

290   **The rate of Ca^{2+} uptake (pumping) (j_{up})** by the SR, based on formulations of SR Ca^{2+} pump

291   function suggested by Luo and Rudy (5). The fractional block (b_{up}) of P_{up} by ChR stimulation

292   was described similar to that of I_{CaL} (see above), but $b_{up,max}$ was fitted to experimental curve of

293   phospholamban dephosphorylation (6) (main text Fig.4A).

294   $$j_{up} = P_{up}/(1 + K_{up}/Ca_i)$$

295   $$P_{up} = P_{up,basal} \cdot (1 - b_{up})$$

296   $$b_{up} = b_{up,max} \cdot [ACh]/(K_{0.5,up} + [ACh])$$

297

298   **Ca^{2+} flux between (network and junctional) SR compartments (j_{tr}):**

299   $$j_{tr} = (Ca_{nSR} - Ca_{jSR})/\tau_{tr}$$

300

301   **Ca^{2+} buffering**

302   $$df_{TC}/dt = k_{fTC} \cdot Ca_i \cdot (1 - f_{TC}) - k_{bTC} \cdot f_{TC}$$

303   $$df_{TMC}/dt = k_{fTMC} \cdot Ca_i \cdot (1 - f_{TMC} - f_{TMM}) - k_{bTMC} \cdot f_{TMC}$$

304   $$df_{TMM}/dt = k_{fTMM} \cdot Mg_i \cdot (1 - f_{TMC} - f_{TMM}) - K_{bTMM} \cdot f_{TMM}$$

305   $$df_{CMi}/dt = k_{fCM} \cdot Ca_i \cdot (1 - f_{CMi}) - k_{bCM} \cdot f_{CMi}$$

306   $$df_{CMs}/dt = k_{fCM} \cdot Ca_{sub} \cdot (1 - f_{CMs}) - k_{bCM} \cdot f_{CMs}$$

307   $$df_{CQ}/dt = k_{fCQ} \cdot Ca_{jSR} \cdot (1 - f_{CQ}) - k_{bCQ} \cdot f_{CQ}$$

308

309   **Dynamics of Ca^{2+} concentrations in cell compartments**

310   $$dCa_i/dt = (j_{Ca\_dif} \cdot V_{sub} - j_{up} \cdot V_{nSR})/V_i - (CM_{tot} \cdot df_{CMi}/dt + TC_{tot} \cdot df_{TC}/dt + TMC_{tot} \cdot df_{TMC}/dt)$$

311   $$dCa_{sub}/dt = j_{SRCarel} \cdot V_{jSR}/V_{sub} - (I_{CaL} + I_{CaT} + I_{bCa} - 2 \cdot I_{NCX})/(2 \cdot F \cdot V_{sub}) - (j_{Ca\_dif} + CM_{tot} \cdot df_{CMs}/dt)$$

312   $$dCa_{jSR}/dt = j_{tr} - j_{SRCarel} - CQ_{tot} \cdot df_{CQ}/dt$$

313   $$dCa_{nSR}/dt = j_{up} - j_{tr} \cdot V_{jSR}/V_{nSR}$$

314

315

316

317 **Online Supplement Table S1.** Model variables: description and initial values. Our SANC model
318 is described by a system of 30 first order differential equations (variables y_1 - y_{30}). All initial
319 values (except that for y_{30}) were taken from our prior study (7).
320

#	Variable	Description	Initial value
		Ca^{2+} cycling	
y_1	Ca_i	$[Ca^{2+}]$ in myoplasm, mM	0.0001
y_2	Ca_{sub}	$[Ca^{2+}]$ in submembrane space, mM	0.000223
y_3	Ca_{jSR}	$[Ca^{2+}]$ in the junctional SR (jSR), mM	0.029
y_4	Ca_{nSR}	$[Ca^{2+}]$ in the network SR (nSR), mM	1.35
y_5	f_{TC}	Fractional occupancy of the troponin-Ca^{2+} site by Ca^{2+} in myoplasm	0.02
y_6	f_{TMC}	Fractional occupancy of the troponin-Mg^{2+} site by Ca^2 in myoplasm	0.22
y_7	f_{TMM}	Fractional occupancy of the troponin-Mg^{2+} site by Mg^{2+} in myoplasm	0.69
y_8	f_{CMi}	Fractional occupancy of calmodulin by Ca^{2+} in myoplasm	0.042
y_9	f_{CMs}	Fractional occupancy of calmodulin by Ca^{2+} in submembrane space	0.089
y_{10}	f_{CQ}	Fractional occupancy of calsequestrin by Ca^{2+} in junctional SR	0.032
y_{11}	R	RyR reactivated (closed) state	0.7499955
y_{12}	O	RyR open state	$3.4 \cdot 10^{-6}$
y_{13}	I	RyR inactivated state	$1.1 \cdot 10^{-6}$
y_{14}	RI	RyR RI state	0.25
		Electrophysiology	
y_{15}	V_m	Membrane potential, mV	-65
y_{16}	d_L	I_{CaL} activation	0
y_{17}	f_L	I_{CaL} voltage-dependent inactivation	1
y_{18}	f_{Ca}	I_{CaL} Ca^{2+} dependent inactivation	1
y_{19}	p_{aF}	I_{Kr} fast activation	0
y_{20}	p_{aS}	I_{Kr} slow activation	0
y_{21}	p_i	I_{Kr} inactivation	1
y_{22}	n	I_{Ks} activation	0
y_{23}	y	I_f activation	1
y_{24}	d_T	I_{CaT} activation	0
y_{25}	f_T	I_{CaT} inactivation	1
y_{26}	q	I_{to} inactivation	1
y_{27}	r	I_{to} and I_{sus} activation	0
y_{28}	q_a	I_{st} activation	0
y_{29}	q_i	I_{st} inactivation	1
y_{30}	a	I_{KACh} activation	1

321

322 **Online Supplement Table S2.**
323 Parameters of steady-state activation and inactivation for I_{CaL} in the present model compared to
324 previous rabbit SANC models (see main text Methods for details). * Steady state inactivation
325 parameters were set in our model to the respective values measured in our laboratory in an
326 experimental study of isolated rabbit SANC by Vinogradova et al. (12).
327

Model	Steady-state activation curve, $d_{L,\infty}$		Steady-state inactivation curve, $f_{L,\infty}$	
	Midpoint, $V_{\frac{1}{2},d}$ (mV)	Slope factor K_d (mV)	Midpoint, $V_{\frac{1}{2},f}$ (mV)	Slope factor K_f (mV)
Wilders et al. (13)	-6.6	6.6	-25	6
Demir et al. (2)	-14.1	6	-25	5
Dokos et al. (3)	-6.6	6.6	-25	6
Zhang et al. (14)	-23.1	6	-45	5
Kurata et al. (4)	-14.1	6	-30	5
Present model	**-13.5**	**6**	**-35***	**7.3***

328
329
330

331 **Online Supplement Table S3.**
332 **Parameter values and result summary of simulations of β-AR stimulation.** In addition to the
333 primary set of model parameters (described above), the robustness of our findings was also
334 tested in two additional model sets (See "Parameter set" column), in which both maximum
335 conductances $g_{CaL,max}$ and $g_{If,max}$ were increased (model set "More I_f & I_{CaL}") or decreased (model
336 set "Less I_f & I_{CaL}") by 25%. While the shift of $V_{If,1/2}$ and relative increases in $g_{CaL,max}$ and $g_{Kr,max}$
337 were set in accordance with previously documented experimental results in rabbis SANC (see
338 main text Methods for details), the values for the maximum Ca^{2+} pumping rate of the SR (P_{up})
339 were found numerically based on parametric sensitivity analyses as solutions to match
340 experimentally documented result of a 25.8% AP firing rate increase (main text figure 2A, black
341 circle, squire, and triangle, respectively).
342
343

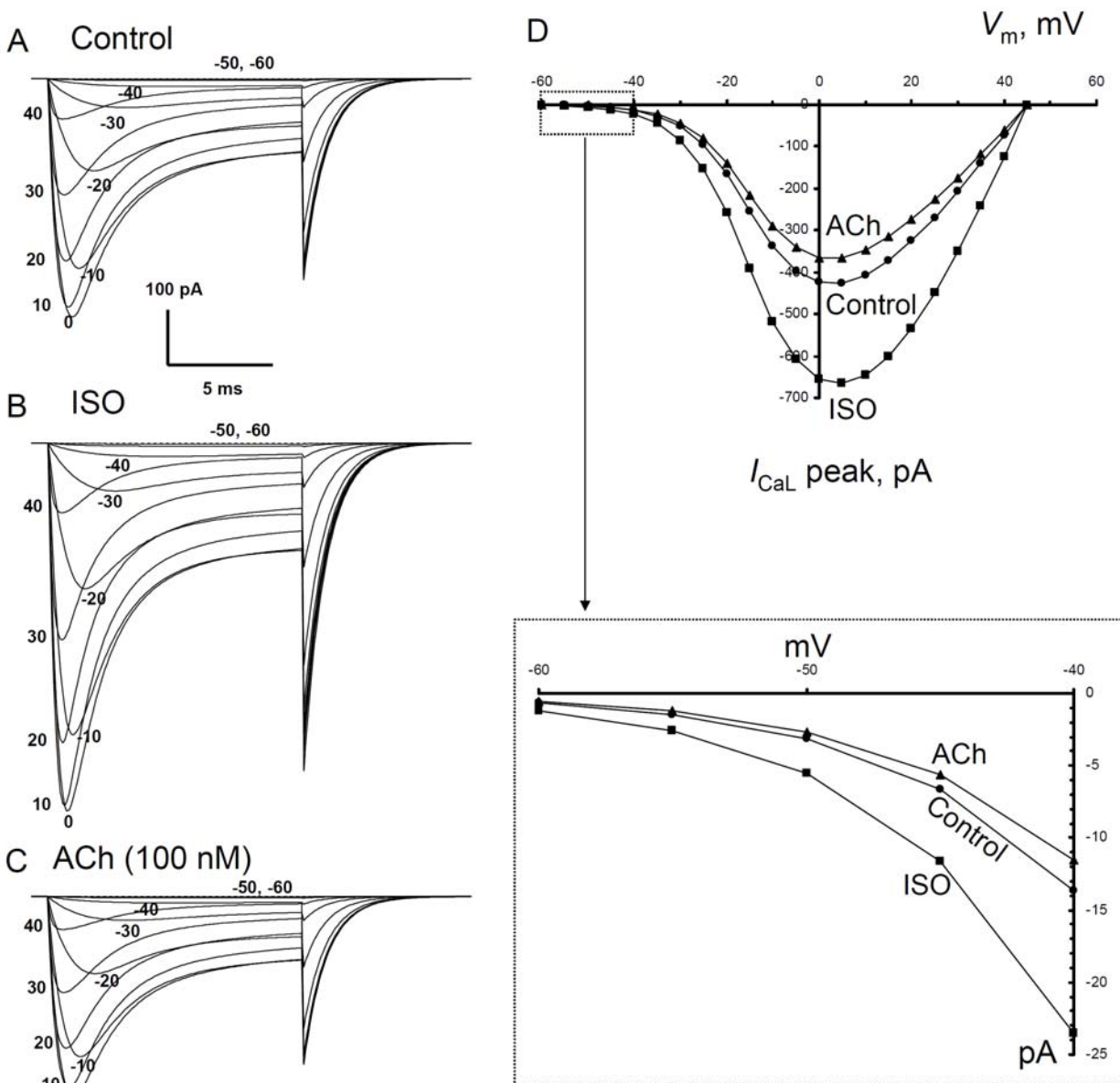| Parameter set	Parameter	Units	Basal state	β-AR stimulation	Effect on beating rate: M clock, only	Effect on beating rate: All mechanisms
Primary model set	P_{up}	mM/s	12	24	3.070 Hz to 3.166 Hz (3.15% increase)	3.070 Hz to 3.862 Hz (25.80% increase)
	$g_{CaL,max}$	nS/pF	0.58	1.015		
	$V_{If,1/2}$	mV	-64	-56.2		
	$g_{Kr,max}$	nS/pF	0.08113973	0.1217096		
	$g_{If,max}$	nS/pF	0.15			
Model set "Less I_f & I_{CaL}"	P_{up}	mM/s	12	20.6	2.943 Hz to 3.089 Hz (4.97% increase)	2.943 Hz to 3.702 Hz (25.80% increase)
	$g_{CaL,max}$	nS/pF	0.435	0.76125		
	$V_{If,1/2}$	mV	-64	-56.2		
	$g_{Kr,max}$	nS/pF	0.08113973	0.1217096		
	$g_{If,max}$	nS/pF	0.1125			
Model set "More I_f & I_{CaL}"	P_{up}	mM/s	12	26.6	3.116 Hz to 3.198 Hz (2.63% increase)	3.116 Hz to 3.920 Hz (25.80% increase)
	$g_{CaL,max}$	nS/pF	0.725	1.26875		
	$V_{If,1/2}$	mV	-64	-56.2		
	$g_{Kr,max}$	nS/pF	0.08113973	0.1217096		
	$g_{If,max}$	nS/pF	0.1875			

344
345
346

347 **Online Supplement Table S4.**
348 **Parameter values and result summary of simulations of ChR stimulation ([ACh[=100 nM).**
349 In addition to the primary set of model parameters (described above), the robustness of our
350 findings was also tested in two additional model sets (See "Parameter set" column), in which
351 both maximum conductances $g_{CaL,max}$ and $g_{If,max}$ were increased (model set "More I_f&I_{CaL}") or
352 decreased (model set "Less I_f&I_{CaL}") by 25%. All parameters, including P_{up}, were calculated
353 using above formulations for [ACh]=100 nM.

354
355

Parameter set	Parameter	Units	Basal state	ChR stimulation	Effect on beating rate M clock	Effect on beating rate M+Ca clock
Primary model set	P_{up}	mM/s	12	7.578947	3.070 Hz to 2.615 Hz (14.8% decrease)	3.070 Hz to 1.849 Hz (40% decrease)
	$g_{CaL,max}$	nS/pF	0.58	0.485368		
	$beta$	ms^{-1}	0	$0.2865116 \cdot 10^{-3}$		
	$V_{If,1/2}$	mV	-64	-69.8089		
	$g_{If,max}$	nS/pF	0.15			
Model set "Less I_f&I_{CaL}"	P_{up}	mM/s	12	7.578947	2.943 Hz to halt	2.943 Hz to halt
	$g_{CaL,max}$	nS/pF	0.435	0.364026		
	$beta$		0	$0.2865116 \cdot 10^{-3}$		
	$V_{If,1/2}$	mV	-64	-69.8089		
	$g_{If,max}$	nS/pF	0.1125			
Model set "More I_f&I_{CaL}"	P_{up}	mM/s	12	7.578947	3.116 Hz to 2.832 Hz (9.1% decrease)	3.116 Hz to 2.354 Hz (24.5% decrease)
	$g_{CaL,max}$	nS/pF	0.725	0.606711		
	$beta$		0	$0.2865116 \cdot 10^{-3}$		
	$V_{If,1/2}$	mV	-64	-69.8089		
	$g_{If,max}$	nS/pF	0.1875			

356
357
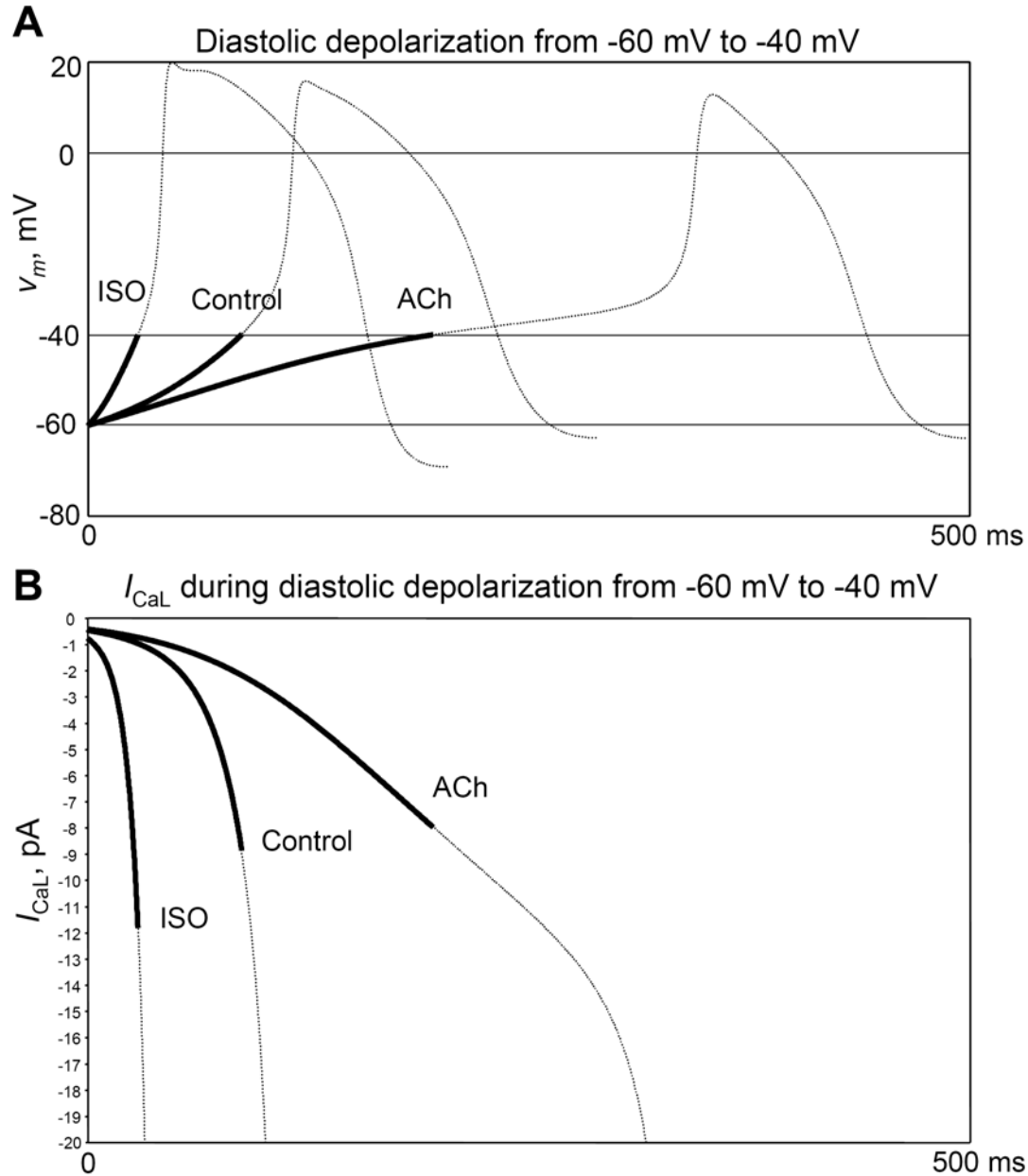358
359

360   **Online Supplement Fig.S1**
361   The predicted effects of GPCR agonists on the current voltage relationship for simulated peak
362   I_{CaL}. The I_{CaL} traces were simulated by applying testing voltage pulses V_m from a holding
363   potential of -80 mV. A, B, and C show simulated traces for V_m from -60 mV to 40 mV with a 10
364   mV interval in the basal state (Control), in the presence of β-AR stimulation by isoproterenol
365   (ISO), and in the presence of ChR stimulation with 100 nM ACh. The values of V_m are shown by
366   labels at the respective current peaks. D: The current voltage relationships (5 mV voltage step)
367   for I_{CaL} peak. Inset illustrates presence of I_{CaL} current activation in the model within the voltage
368   range of the diastolic depolarization from -60 mV to -40 mV. Cell electric capacitance is 32 pF.

369
370

371   **Online Supplement Fig.S2**
372   The predicted effects of GPCR agonists on I_{CaL} dynamics during diastolic depolarization (DD)
373   from -60 mV to -40 mV. A: simulated action potentials (APs) in the basal state (Control), in
374   the presence of β-AR stimulation by isoproterenol (ISO), and in the presence of ChR stimulation
375   with 100 nM ACh. APs were time shifted to overlap at -60 mV. DD fragments from -60 to -40
376   mV are shown by solid black curves. B: simultaneously simulated dynamics of I_{CaL}. Activation
377   of I_{CaL} accelerated and increased in case of ISO but decelerated and decreased in case of ACh.
378   Cell electric capacitance is 32 pF.
379

380

381   Supplemental references
382
383
384

385   1.   **Demir SS, Clark JW, and Giles WR.** Parasympathetic modulation of sinoatrial node
386   pacemaker activity in rabbit heart: a unifying model. *Am J Physiol* 276: H2221-2244, 1999.
387   2.   **Demir SS, Clark JW, Murphey CR, and Giles WR.** A mathematical model of a rabbit
388   sinoatrial node cell. *Am J Physiol* 266: C832-852, 1994.
389   3.   **Dokos S, Celler B, and Lovell N.** Ion currents underlying sinoatrial node pacemaker
390   activity: a new single cell mathematical model. *J Theor Biol* 181: 245-272, 1996.
391   4.   **Kurata Y, Hisatome I, Imanishi S, and Shibamoto T.** Dynamical description of
392   sinoatrial node pacemaking: improved mathematical model for primary pacemaker cell. *Am
393   J Physiol* 283: H2074-2101, 2002.
394   5.   **Luo CH and Rudy Y.** A dynamic model of the cardiac ventricular action potential. I.
395   Simulations of ionic currents and concentration changes. *Circ Res* 74: 1071-1096, 1994.
396   6.   **Lyashkov AE, Vinogradova TM, Zahanich I, Li Y, Younes A, Nuss HB, Spurgeon
397   HA, Maltsev VA, and Lakatta EG.** Cholinergic receptor signaling modulates spontaneous
398   firing of sinoatrial nodal cells via integrated effects on PKA-dependent Ca^{2+} cycling and
399   I_{KACh}. *Am J Physiol Heart Circ Physiol*: H949-H959, 2009.
400   7.   **Maltsev VA and Lakatta EG.** Synergism of coupled subsarcolemmal Ca^{2+} clocks and
401   sarcolemmal voltage clocks confers robust and flexible pacemaker function in a novel
402   pacemaker cell model. *Am J Physiol Heart Circ Physiol* 296: H594-H615, 2009.
403   8.   **Sakai R, Hagiwara N, Matsuda N, Kassanuki H, and Hosoda S.** Sodium--potassium
404   pump current in rabbit sino-atrial node cells. *J Physiol* 490 (Pt 1): 51-62, 1996.
405   9.   **Shannon TR, Wang F, Puglisi J, Weber C, and Bers DM.** A mathematical treatment of
406   integrated Ca dynamics within the ventricular myocyte. *Biophys J* 87: 3351-3371, 2004.
407   10.   **Shinagawa Y, Satoh H, and Noma A.** The sustained inward current and inward rectifier
408   K^+ current in pacemaker cells dissociated from rat sinoatrial node. *J Physiol* 523 Pt 3: 593-
409   605, 2000.
410   11.   **Stern MD, Song LS, Cheng H, Sham JS, Yang HT, Boheler KR, and Rios E.** Local
411   control models of cardiac excitation-contraction coupling. A possible role for allosteric
412   interactions between ryanodine receptors. *J Gen Physiol* 113: 469-489, 1999.
413   12.   **Vinogradova TM, Zhou YY, Bogdanov KY, Yang D, Kuschel M, Cheng H, and Xiao
414   RP.** Sinoatrial node pacemaker activity requires Ca^{2+}/calmodulin-dependent protein kinase
415   II activation. *Circ Res* 87: 760-767, 2000.
416   13.   **Wilders R, Jongsma HJ, and van Ginneken AC.** Pacemaker activity of the rabbit
417   sinoatrial node. A comparison of mathematical models. *Biophys J* 60: 1202-1216, 1991.
418   14.   **Zhang H, Holden AV, Kodama I, Honjo H, Lei M, Varghese T, and Boyett MR.**
419   Mathematical models of action potentials in the periphery and center of the rabbit sinoatrial
420   node. *Am J Physiol* 279: H397-421, 2000.
421   15.   **Zhang H, Holden AV, Noble D, and Boyett MR.** Analysis of the chronotropic effect of
422   acetylcholine on sinoatrial node cells. *J Cardiovasc Electrophysiol* 13: 465-474, 2002.
423
424